Original Research Paper

Gp350-anchored extracellular vesicles: promising vehicles for delivering therapeutic drugs of B cell malignancies

Huiqing Xiu [a,#], *Xi Nan* [a,#], *Danfeng Guo* [b,#], *Jiaoli Wang* [c,d,#], *Jiahui Li* [e], *Yanmei Peng* [a], *Guirun Xiong* [f], *Shibo Wang* [a], *Changjun Wang* [g], *Gensheng Zhang* [e,*], *Yunshan Yang* [h,*], *Zhijian Cai* [a,*]

[a] *Institute of Immunology, and Department of Orthopedics of the Second Affiliated Hospital, Zhejiang University School of Medicine, Hangzhou, China*

[b] *Henan Key Laboratory for Digestive Organ Transplantation, the First Affiliated Hospital of Zhengzhou University, Zhengzhou, China*

[c] *Key Laboratory of Clinical Cancer Pharmacology and Toxicology Research of Zhejiang Province, Affiliated Hangzhou First People's Hospital, Zhejiang University School of Medicine, Hangzhou, China;*

[d] *Zhejiang University Cancer Centre, Hangzhou, China*

[e] *Department of Critical Care Medicine of the Second Affiliated Hospital, Zhejiang University School of Medicine, Hangzhou, China*

[f] *Department of Emergency Medicine, Tongde Hospital of Zhejiang Province, Hangzhou, China*

[g] *Second Affiliated Hospital of Zhejiang University School of Medicine, Zhejiang Provincial Key Lab of Ophthalmology, Hangzhou, China*

[h] *Department of Medical Oncology, The Cancer Hospital of the University of Chinese Academy of Sciences (Zhejiang Cancer Hospital), Institute of Basic Medicine and Cancer (IBMC), Chinese Academy of Sciences, Hangzhou, China.*

A R T I C L E   I N F O

A B S T R A C T

Although chimeric antigen receptor-modified (CAR) T cell therapy has been successfully applied in the treatment of acute B lymphocytic leukemia, its effect on Burkitt lymphoma (BL) and chronic B lymphocytic leukemia (B-CLL) is unsatisfactory. Moreover, fatal side effects greatly impede CAR T cell application. Extracellular vesicles (EVs) are excellent carriers of therapeutic agents. Nevertheless, EVs mainly accumulate in the liver when administered without modification. As an envelope glycoprotein of Epstein–Barr viruses, gp350 can efficiently bind CD21 on B cells. Here, gp350 was directly anchored onto red blood cell EVs (RBC-EVs) via its transmembrane region combined with low-voltage electroporation. The results showed that gp350 could anchor to RBC-EVs with high efficiency and that the resulting gp350-anchored RBC-EVs (RBC-EVs/gp350^{Etp}) exhibited increased targeting to CD21$^+$ BL and B-CLL relative to RBC-EVs. After the loading of doxorubicin or fludarabine, RBC-EVs/gp350^{Etp} had powerful cytotoxicity and therapeutic efficacy on CD21$^+$ BL or B-CLL, respectively. Moreover, RBC-EVs/gp350^{Etp} loaded with a drug did not exhibit any apparent systemic toxicity and specifically induced the apoptosis of tumor B cells but not normal B

---

cells. Therefore, our findings indicate that drug-loaded RBC-EVs/gp350^{Etp} may be adopted in the treatment of CD21$^+$ B cell malignancies.

1. Introduction

At present, chimeric antigen receptor-modified (CAR) T cell therapy is considered advanced, and studies have shown CD19 is a perfect target for this therapy in most B cell malignancies [1,2]. The therapy has attained impressive outcomes in individuals with acute B lymphocytic leukemia (B-ALL) [3]. Although it exerts some effects in diffuse large B cell lymphoma [4], the effects of this therapy on Burkitt lymphoma (BL) remain unclear [5], and the function of CAR T cell therapy in chronic B lymphocytic leukemia (B-CLL) is limited [6]. Dysfunctional CAR T cells and increased modulatory T cells in patients with B-CLL probably blunt the efficacy of CAR T cells [7,8]. In addition, notable toxicities, such as cytokine release syndrome of CAR T cells, will threaten patients' lives [9]. Therefore, the therapy of B cell malignancies, particularly BL and B-CLL, remains challenging [10,11].

Extracellular vesicles (EVs), including ectosomes, exosomes, oncosomes, and apoptotic bodies, are membranous vesicles released by various cells that can transfer messages between cells [12,13]. The feasibility and advantages of EVs as drug carriers have been verified in many studies [14,15]. EVs can not only carry proteins [16], noncoding RNAs [17], CRISPR–Cas9 plasmids [18] and chemotherapy drugs [19] but also protect these cargoes from degradation and thereby enhance their therapeutic efficacy. Compared with liposomes, which are extensively studied drug delivery vehicles, EVs are natural nanoparticles of cells with lower immunogenicity and cytotoxicity as well as better permeability [20,21]. EVs from mesenchymal cells can carry *Kras* siRNA or shRNA to effectively suppress pancreatic cancer [22]. Super-repressor IκB-loaded EVs improve survival in an LPS-induced septic mouse model [23], and EVs encapsulating chemotherapeutic drugs such as doxorubicin (Dox) exert excellent therapeutic effects on murine cancer without obvious toxicity [19].

Despite numerous explorations, the clinical translation of EVs as drug carriers remains challenging. For clinical treatment, the EV source is a critical issue to consider. Red blood cell EVs (RBC-EVs) are promising candidates due to their high yield and ideal safety [24]. However, our previous study demonstrated that most unmodified RBC-EVs naturally accumulate in the liver, which greatly restricts their output efficiency for therapeutic drugs of diseases beyond the liver [25]. Thus, endowing EVs with targeting properties would be meaningful. Epstein–Barr virus (EBV) primarily infects human B cells by interacting with the envelope glycoprotein gp350 and CD21 [26]. Exosomes from EBV-transformed B cells containing gp350 can block EBV infection by selectively targeting mature B cells via the gp350-CD21 interaction [27]. Gp350-containing EVs are B cell tropic and can transfer neoantigens to B cell malignancies [28]. Therefore, gp350-modified EVs are probably optimized vehicles for the delivery of therapeutic drugs to B cell malignancies via CD21.

In this study, gp350 was effectively anchored onto RBC-EVs via the transmembrane (TM) region through low-voltage electroporation, and the resulting gp350-anchored RBC-EVs (RBC-EVs/gp350^{Etp}) showed stronger targeting to tumor CD21$^+$ B cells than RBC-EVs. Dox is a common and effective drug used for the treatment of BL [29], and fludarabine (FA) is a nucleoside analog of cytarabine that affects DNA synthesis and has been effectively used for CLL treatment [30]. Correspondingly, after loading with Dox or FA, RBC-EVs/gp350^{Etp} showed increased cytotoxicity to tumor CD21$^+$ B cells and significantly inhibited the progression of BL or B-CLL, respectively. However, RBC-EVs/gp350^{Etp} loaded with Dox or FA did not lead to systemic toxicity. Therefore, our results demonstrate that the generated EVs are potential therapeutic reagents for CD21$^+$ BL and B-CLL.

2. Materials and methods

2.1. Mouse samples and human samples

Joint Ventures Sipper BK Experimental Animal Co. (Shanghai, China) provided male 6–8-week-old C57BL/6J and BALB/c-nude mice, and the Model Animal Research Center of Nanjing University (Nanjing, Jiangsu, China) offered male NCG (NOD-*Prkdc^{em26Cd52}Il2rg^{em26Cd22}*/Nju) mice aged 6–8 weeks. All the mice were maintained in a pathogen-free facility and cared for in accordance with the institution guidelines, and the experiment was approved by the Animal Care and Use Committee of Zhejiang University (ZJU20210089). Fifteen healthy type O blood donors provided human blood (50 ml/donor), were informed of the usage of their blood, and signed consent forms. The local Ethical Committee and the Review Board of Zhejiang University approved the human blood collection (2021-045).

2.2. Cell lines

293T cells, the human B-ALL cell line SupB15, and the human B-CLL cell line MEC-1 were provided by the American Type Culture Collection (Manassas, VA, USA). The human chronic myeloid leukemia cell line K562 and the human BL cell line Raji were purchased from the Chinese Academy of Sciences. Luciferase-expressing MEC-1 (MEC-1-Luci) cells were established in the laboratory according to a previous publication [25], and 293T cells were kept in DMEM containing 10% fetal bovine serum (FBS) and penicillin/streptomycin at a concentration of 1%. K562, SupB15, Raji and MEC-1 cells were maintained in IMDM under the same conditions. All the

cells were incubated at 37 degrees Celsius in a humidified environment with 5% CO_2. A Mycoplasma Detection Kit (Lonza, Basel, Switzerland) was used to test all the cells for mycoplasma contamination, and the results were all negative. Shanghai Biowing Applied Biotechnology (Shanghai, China) authenticated these cell lines through DNA short-tandem repeat analysis.

2.3. Plasmid construction and transfection

The gp350 gene was synthesized by Sanyou Bio (Shanghai, China) and inserted into a pCDNA3.0-Flag (Invitrogen, New York, USA) or pET28a (Miaoling, Shanghai, China) plasmid using endonucleases and T4 ligase (TaKaRa, Dalian, Liaoning, China). PEI reagent (Polysciences, Pennsylvania, USA) was utilized for the transfection of 293T cells with pCDNA3.0-gp350-Flag based on the manufacturer's guidance.

2.4. Isolation of EVs

We separated the RBCs from the white blood cells and plasma through a 10-min centrifugation at $500 \times g$ and passed the solution through a leukodepletion filter. We diluted the separated RBCs in dilution medium (20.5 g/l glucose, 4.2 g/l NaCl, 2 mM $CaCl_2$) and treated the RBCs with 10 µM calcium ionophore (Sigma–Aldrich, St. Louis, MO, USA) overnight at 37 degrees Celsius. Afterward, the RBCs and cell debris were removed through a 20-min centrifugation at $600 \times g$, a 15-min centrifugation at $1600 \times g$, a 15-min centrifugation at $3260 \times g$, and a 30-min centrifugation at $10\,00 \times g$ at 4 degrees Celsius. For the isolation of 293T cell EVs, the culture supernatants of the cells were differentially centrifuged through a 10-min centrifugation at $300 \times g$, a 20-min centrifugation at $2000 \times g$, and a 30-min centrifugation at $10\,000 \times g$ at 4 degrees Celsius. The solution was then passed through 0.22-µm syringe filters and subjected to a 70-min ultracentrifugation at $100\,000 \times g$ at 4 degrees Celsius. The pellets were rinsed with a large amount of ice-cold PBS and centrifuged at $100\,000 \times g$ and 4 degrees Celsius for an additional 70 min. The final pellets were resuspended in PBS. The EV protein concentrations were analyzed using a BCA Protein Assay Kit (Thermo Fisher Scientific).

2.5. Electron microscopy and nanoparticle analysis

We placed 5 µg EVs on 200-mesh copper grids coated with carbon at room temperature (RT) for 2 min. The excess suspension was removed using filter paper. The EVs were negatively stained with uranyl acetate at RT for 5 min, washed twice with PBS and subjected to a drying treatment. The EVs were measured under an FEI Tecnai T10 electron microscope (FEI, Hillsboro, OR, USA) running at 120 kV, and images were obtained. The EV grain distribution was assayed using a NanoSight NS500 instrument (Malvern, Malvern, Worcestershire, UK).

2.6. Western blotting

Ten micrograms EVs, cell lysate proteins or tumor tissues were separated via SDS–PAGE in 10% gels and transferred onto polyvinylidene difluoride membranes. The membranes were blocked with 5% powdered skim milk in PBST buffer, incubated with related primary antibodies overnight at 4 degrees Celsius and incubated with horseradish peroxidase-conjugated secondary antibodies for 1 h. Enhanced chemiluminescence reagents (MultiSciences, Hangzhou, Zhejiang, China) and a Tanon 4500 Gel Imaging System were utilized to detect the bands. Table S1 shows the informations of antibodies used in the assay and their corresponding dilutions.

2.7. Protein expression and purification

Purification of gp350 was performed according to a previous report [31]. Briefly, the gp350-His-pET28a vector was selected for transformation into the BL21(DE3) strain of E. coli (TsingKe Biotech, Beijing, China). The transformed cells with kanamycin resistance were placed on LB plates containing kanamycin and incubated overnight at 37 degrees Celsius. A single colony was then selected from the plate and cultured in 20 ml LB overnight. The obtained BL21 (DE3)-gp350 culture was adopted for grafting in 300 ml LB with violent shaking at 37 degrees Celsius. As soon as the OD600 reached 0.8, 1 mM isopropyl-beta-D-thiogalactopyranoside (IPTG, Beyotime, Shanghai, China) was added, and the mixture was incubated at 24 degrees Celsius for 12 h to trigger protein overexpression. Protein-expressing bacteria were harvested by centrifugation and washed three times with PBS. These pellets were dissolved in lysis buffer (50 mM Tris, 300 mM NaCl, 0.2 mM PMSF, 0.1% Triton X-100, pH 7.8) and lysed using an ultrasonic cell disruptor (power: 400 W; mode: on for 5 s and off for 5 s over a 20-min period) (#DH92-IIN, LAWSON, China). The prepared solution underwent a 20-min centrifugation at 20 000 g. We collected the supernatants and mixed them with pre-equilibrium nickel beads (Sangon, Shanghai, China) for 6 h at 4 degrees Celsius. The column was rinsed with urea/SDS buffer, and the proteins were eluted with 250 mM imidazole (Solarbio, Beijing, China). The final fractions were collected, and SDS–PAGE and Coomassie staining confirmed the purity of the protein.

2.8. SiRNA transfection

Raji cells were transfected with scrambled negative control (NC) or Cd21 siRNA using INTERFERin siRNA Transfection reagent (Polyplus, Beijing, China) according to the manufacturer's instructions. The effects of gene silencing were then measured by quantitative PCR (qPCR) and flow cytometry. The siRNAs were synthesized by GenePharma. The sequences and primers used are listed in Table S2.

2.9. RBC-EV electroporation

RBC-EV electroporation was conducted with a BTX electroporator (Harvard Biosciences, Cambridge, MA, USA). To load the EVs with Dox (Haizheng Pharmaceuticals, Zhejiang, China) or FA (Haizheng Pharmaceuticals, Zhejiang, China), 100 µg RBC-EVs and 100 µg Dox or 500 µg FA were lightly blended and incubated at 37 degrees Celsius for 60 min. After electroporation at 150 µF and 350 V in 2-mm electroporation

cuvettes, the mixture was incubated at 37 degrees Celsius for 30 min to ensure complete recovery of the EV plasma membrane. To remove unincorporated Dox or FA, the EVs were rinsed twice with PBS before ultracentrifugation at $120\,000 \times g$ for 90 min. The drug-loaded EVs were broken by ultrasonication (60 cycles of 10 s on and 10 s off, 35% efficacy) and centrifuged at $120\,000 \times g$ for 90 min. The Dox or FA concentration was measured utilizing a previously described LC–MS/MS approach [32,33].

2.10. Anchorage of gp350 onto RBC-EVs

To incorporate gp350 proteins onto RBC-EVs, 100 µg RBC-EVs or drug-loaded RBC-EVs were incubated with 50 µg purified gp350 proteins for 60 min at 37 degrees Celsius and then electroporated at 50 V and 100 µF in 2-mm electroporation cuvettes utilizing a Gene Pulser Xcell electroporator (Bio–Rad, Hercules, CA, USA). Unbound gp350 proteins were removed with an Ultrafree 0.5 Biomax 100 K filter during a 20-min centrifugation at $4000 \times g$ (Millipore, Bedford, USA), and the remaining RBC-EVs/gp350^{Etp} were rinsed and collected in PBS.

2.11. Labeling and tracking of EVs

We labeled EVs with a VivoTrack 680 (Fluorescence, Beijing, China), PKH26, (Sigma–Aldrich) based on the manufacturer's guidance. For VivoTrack 680 labeling, we mixed 100 µg RBC-EVs in 100 µl PBS with 30 µM VivoTrack 680 at RT for 30 min. For PKH26 labeling, we resuspended 50 µg EVs in 100 µl diluent C, and 2 µl PKH26 or PKH67 dye solution was added to a separate volume of diluent C containing the same amount. Afterward, 100 µl the EV suspension was mixed with 100 µl the dye solution for 5 min. For CFSE labeling, we incubated 50 µg EVs in 100 µl PBS with 7.5 µM CFSE at 37 degrees Celsius for 10 min. The staining was terminated by the addition of 100 µl FBS (EV-depleted, Thermo Fisher Scientific) and further incubation for 3 min. Ultimately, all the free dye was eliminated through a 90-min ultracentrifugation at $100\,000 \times g$, and the pellets were resuspended in 200 µl PBS An *in vivo* imaging system (IVIS, PerkinElmer, Waltham, MA, USA) was used to image the uptake of VivoTrack 680-labeled EVs.

2.12. Flow cytometric analysis

To conduct this analysis, EVs were coated onto 4-µm-diameter aldehyde-sulfate latex beads (Thermo Fisher Scientific), as previously described [34]. We incubated 10 µg EVs with 10 µl beads for 30 min at RT in PBS. The mixture then underwent blockage by incubation with 50 µl FBS (depleted of EVs) for 30 min. After two washes with PBS, the beads coated with EVs were stained with the related antibodies labeled with fluorescence for 30 min at 4 degrees Celsius. For the surface staining of cells, the cells were rinsed twice with PBS and incubated with the related fluorescent antibodies for 30 min on ice. After three washes with PBS, the beads or cells were analyzed via flow cytometry (NovoCyte flow cytometer, Agilent Biosciences, San Diego, CA, USA). A flow cytometric analysis of apoptotic cells was conducted by staining the cells utilizing an Annexin V-PI Apoptosis Detection Kit (MultiSciences) based on the manufacturer's guidance. We

analyzed the data using FlowJo software (Tree Star, Ashland, OR, USA). Table S1 provides the antibodies used in this study and detailed information.

2.13. Cell viability assay

The viability of Raji, K562, MEC-1 and SupB15 cells was measured through CCK-8 assays (TransGen, Beijing, China) based on the manufacturer's protocol. The cells were treated with 10 µg/ml RBC-EVs, RBC-EVs/Dox, RBC-EVs/FA, RBC-EVs/gp350^{Etp}/Dox, RBC-EVs/gp350^{Etp}/FA, Dox (0.3 or 5 µg/ml) or FA (1.7 or 10 µg/ml) for 24 h, 48 h and 96 h in a 96-well plate, and after 10 µl CCK-8 reagent (TransGen, Beijing, China) was added to each well, the plates were incubated for 2 h at 37 degrees Celsius. The absorbance at 450 nm, which reflected the cell viability, was determined with a microplate reader.

2.14. Tumor models and treatments

We subcutaneously (s.c.) injected male BALB/c-nude mice with 1×10^7 Raji or K562 cells on Day 0. The mice with tumors were randomized and intravenously (i.v.) injected with 100 µg RBC-EVs/Dox, RBC-EVs or RBC-EVs/gp350^{Etp}/Dox or a routine dose of Dox (RD/Dox, 5 mg/kg) every 3 d after the tumors reached 100 mm^3. We monitored the tumor size every other day with a Vernier caliper. For development of a B-CLL mouse model, 2×10^6 MEC-1-Luci cells were injected i.v. into NCG mice, and 8 d later, the mice with tumors were randomized and injected i.v. with 100 µg RBC-EVs, RBC-EVs/FA, or RBC-EVs/gp350^{Etp}/FA or a routine dose of FA (RD/FA, 25 mg/kg) every 3 d. The mice were imaged with an IVIS on a regular basis. For analyses of the tumor burden, the tumors were analyzed using Living Image version 4.4 software (Caliper Life Sciences).

2.15. Immunofluorescence

Tumors were collected after treatment for 10 d, embedded in Tissue-Tek Cryo-O.C.T. compound (Thermo Fisher Scientific) and cut to obtain 4-µm sections. The resulting small tumor pieces were fixed, stained with the indicated primary antibodies overnight at 4 degrees Celsius, and then stained with the related fluorescence-labeled secondary antibodies at RT for 30 min. The nuclei were then stained with DAPI for 20 min at RT. An Olympus FV3000 confocal microscope was utilized to observe the stained sections. Table S1 lists the antibodies used in this study and their corresponding dilutions.

2.16. TUNEL analysis

The TUNEL assay was conducted using the TUNEL detection kit (TUNEL, Beyotime) according to the instructions. Briefly, tumors were collected after treatment for 10 d, embedded in Tissue-Tek Cryo-O.C.T. compound (Thermo Fisher Scientific) and cut to obtain 4-µm sections. The slices were fixed in 4% paraformaldehyde at RT for 30 min. After two washes with PBS, the samples were treated with 0.3% Triton X-100 for 15 min. Subsequently, 50 µl the TUNEL reaction mixture (5 µl TdT enzyme solution and 45 µl labeling solution) was added,
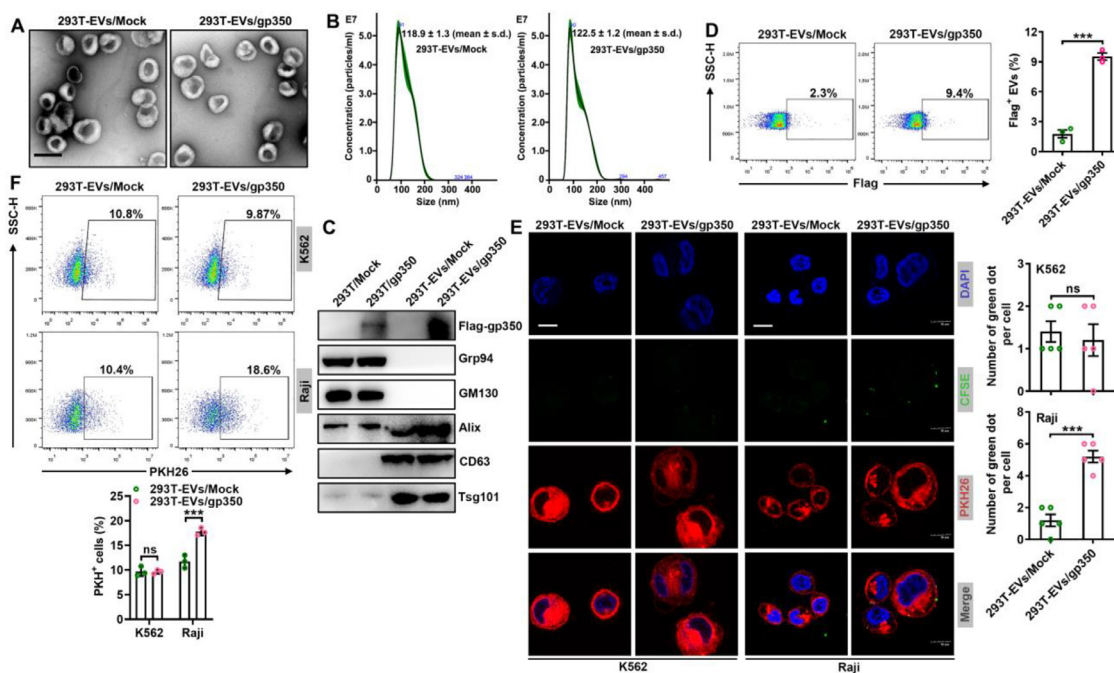
Fig. 1 – Modification with gp350 increases the uptake of 293T-EVs by tumor CD21+ B cells. (A-D) Mock or *Flag-gp350* overexpression plasmids were transfected into 293T cells, and 48 h later, EVs were separated from the supernatants of these cells. The EV morphology was detected by TEM. Scale bar, 100 nm (A). The EV grain distribution was detected using nanoparticle tracking analysis (B). The indicated proteins in the EVs were detected by immunoblotting (C). Flow cytometry was applied to analyze flag-gp350 proteins on the EVs (D). (E) PKH26-labeled K562 or Raji cells were incubated with CFSE-labeled 293T-EVs/Mock or 293T-EVs/gp350 (10 µg/ml) at 4 degrees Celsius for 1 h, and the EVs on the cells were then detected by fluorescence microscopy. Scale bar, 10 µm. (F) Raji or K562 cells were maintained with 10 µg/ml PKH26-labeled 293T-EVs/Mock or 293T-EVs/gp350 at 37 degrees Celsius for 1 h, and the EV uptake was then detected by flow cytometry. ns: not significant; ***$P < 0.001$ (unpaired Student's t test). Typical outcomes from three independent trials are given (mean ± SD) ($n = $ 3-5).

and the resulting mixture was incubated for 1 h at 37 degrees Celsius in a dark humidified environment. The cells were costained with DAPI and visualized with an Olympus FV3000 confocal microscope.

2.17. Histopathology

The liver, spleen, heart, kidneys and lungs from a single mouse of each of the various groups were separated after treatment for 18 d, briefly fixed in 4% paraformaldehyde and subjected to hematoxylin and eosin (H&E) staining.

2.18. Blood biochemistry

Mouse blood was collected in ethylenediaminetetraacetic acid-containing tubes (Xiangyuan Medical Apparatus Co. Ltd., Shijiazhuang, Hebei, China) to prevent coagulation and analyzed using an ADVIA 2120 automatic hematological analyzer (Siemens, Erlangen, Germany) and an ADVIA 2400 automatic biochemistry analyzer (Siemens). The analytical measurements included a routine blood count (leukocyte and RBC levels) and assessment of the lactate dehydrogenase (LDH) and creatine kinase isoenzyme-MB (CK-MB) levels in sera.

2.19. Determination of cytokine levels

The murine serum IL-6, IL-1β and TNF levels were detected by ELISA (BioLegend, San Diego, CA, USA) based on the manufacturer's guidance.

2.20. Isolation of CD21+ lymphocytes

Human peripheral blood mononuclear cells were isolated using lymphocyte separation medium (Haoyang bio, Tianjin, China) according to the manufacturer's guidance. For the isolation of CD21+ lymphocytes from human peripheral blood mononuclear cells, CD21+ cells were further sorted with a Beckman MoFlo Astrios EQ (Beckman Coulter).

2.21. Statistical analyses

The data are expressed as the means and standard deviations (SD). The significance of the average differences between two groups was assessed using an unpaired Student's t test, and the significance of the differences among various groups was evaluated by one-way ANOVA followed by Newman–Keuls multiple comparison test. We performed survival analyses using log-rank tests. GraphPad Prism 8.0.2 (GraphPad Software

Inc., San Diego, CA, USA) software was applied for the analyses, and a $P < 0.05$ was considered to indicate statistical significance.

3. Results and discussion

3.1. Modification with gp350 increases the uptake of 293T-EVs by tumor CD21$^+$ B cells

To obtain EVs with membrane gp350, we transfected mock plasmids or plasmids encoding the full-length *gp350* gene, including the TM sequence, into 293T cells (termed 293T/Mock and 293T/gp350, respectively) and confirmed the overexpression of gp350 proteins (Fig. S1A). We then isolated the secreted EVs from these cells (termed 293T-EVs/Mock and 293T-EVs/gp350, respectively) and confirmed that these two EVs were mainly 100 nm in diameter and had a classic two-layer membrane structure (Fig. 1A). The grain distribution analysis showed that the average sizes of the 293T-EVs/Mock and 293T-EVs/gp350 were 118.9 ± 1.3 nm and 122.5 ± 1.2 nm, respectively (Fig. 1B). Furthermore, both EVs were positive for the EV markers Alix, CD63 and Tsg101 and negative for the endoplasmic reticulum-residing protein GRP94 and the Golgi protein GM130, but only 293T-EVs/gp350 were positive for gp350 (Fig. 1C). Flow cytometry further confirmed the existence of membrane gp350 on the surface of 293T-EVs/gp350, although at insignificant levels (Fig. 1D). Subsequently, we examined whether 293T-EVs/gp350 had an increased ability to target CD21$^+$ B cells. CFSE-labeled EVs were incubated at 4 degrees Celsius with PKH26-labeled CD21$^+$ Raji cells or CD21$^-$ K562 cells (Fig. S1B). In comparison with the levels of 293T-EVs/Mock, increased levels of 293T-EVs/gp350 were observed on the surface of Raji but not K562 cells (Fig. 1E), which suggested enhanced binding of gp350-modified EVs to CD21$^+$ cells. Consistent with these results, we found that Raji but not K562 cells took up more PKH26-labeled 293T-EVs/gp350 than 293T-EVs/Mock during incubation at 37 degrees Celsius (Fig. 1F). These data suggest that the gp350 modification effectively enhances the targeting of EVs to tumor CD21$^+$ B cells.

3.2. Successful anchorage of gp350 onto RBC-EVs via the TM region plus low-voltage electroporation

The efficiency of the loading of gp350 on 293T-EVs through the overexpression of gp350 in 293T cells was low. Moreover, as ideal EV source cells, RBCs cannot express exogenous proteins due to a lack of transcription systems [24,25]. Therefore, we wanted to directly anchor gp350 onto RBC-EVs. Superantigen SEA proteins with TM domains can effectively anchor to EVs through direct *in vitro* incubation [35]. In addition, electroporation is widely used for the encapsulation of cargoes into EVs [36]. Thus, we hypothesized that gp350 could be anchored on RBC-EVs through simple *in vitro* incubation and that electroporation might expand the spacing between membrane lipids and thereby further improve the anchoring efficiency. We confirmed that purified gp350 had the ability to more strongly bind to CD21$^+$ Raji than CD21$^-$ K562 cells

(Fig. S2A). We then found that simple *in vitro* incubation indeed resulted in the anchorage of gp350 onto RBC-EVs (RBC-EVs/gp350) (Fig. 2A and 2B). In addition, the combination of incubation with low-voltage electroporation significantly enhanced the anchoring efficiency of gp350 onto RBC-EVs (RBC-EVs/gp350^{Etp}) (Fig. 2A and 2B). We then confirmed that the optimal voltage for RBC-EV electroporation was low (50 V) and that the optimal mass ratio of EVs to gp350 was 100 μg to 50 μg (Fig. S2B and S2C). After incubation with proteinase K, gp350 was no longer detected on RBC-EVs/gp350^{Etp} by flow cytometry (Fig. 2C), which further supported the membrane anchorage of gp350. In addition, gp350 could not be detected in proteinase K-treated EVs by western blotting (Fig. 2D), which indicated that low-voltage electroporation did not pack gp350 into RBC-EVs. The analysis also confirmed that low-voltage electroporation did not obviously alter the morphology and grain distribution of RBC-EVs (Fig. S2D and S2E). Furthermore, both EVs were positive for the RBC marker hemoglobin A1 and the EV markers Alix and Tsg101 (Fig. S2F). To roughly evaluate the stability of gp350 anchorage *in vitro*, we preserved RBC-EVs/gp350^{Etp} at 37 degrees Celsius and discovered that the anchorage was stable for at least 3 d (Fig. 2E). Therefore, the combination of incubation with low voltage can directly anchor gp350 onto RBC-EVs with high efficiency.

3.3. RBC-EVs/gp350^{Etp} exhibit enhanced targeting to tumor CD21$^+$ B cells

We then tested the targeting of RBC-EVs/gp350^{Etp} to tumor CD21$^+$ B cells. The amounts of RBC-EVs/gp350^{Etp} taken up by Raji cells and CD21$^+$ MEC-1 cells (Fig. S3A) were higher than those of RBC-EVs (Fig. 3A and 3B). However, the uptake of both EVs by CD21$^-$ K562 and SupB15 cells did not differ (Fig. S3B and S3C). To further confirm the role of CD21 in this process, we knocked down *Cd21* in Raji cells and found that *Cd21* knockdown greatly reduced the uptake of RBC-EVs/gp350^{Etp} by Raji cells (Fig. S3D and S3E). We then assessed the CD21$^+$ tumor targeting ability of RBC-EVs/gp350^{Etp} *in vivo*. Consistent with their ability to target CD21$^+$ cells, RBC-EVs/gp350^{Etp} showed higher accumulation in Raji tumors and less accumulation in the liver than RBC-EVs (Fig. 3C). However, both EVs showed similar accumulation in K562 tumors (Fig. 3C). These results were further confirmed by tissue fluorescence detection (Fig. 3D and S3F). To test whether gp350 anchorage could also increase the targeting of EVs to CD21$^+$ hematologic malignancies, we established CD21$^+$ MEC-1 and CD21$^-$ SupB15 leukemia cells in NCG mice. Similarly, MEC-1 cells took up more RBC-EVs/gp350^{Etp} than RBC-EVs, and this finding could not be obtained with SupB15 leukemia (Fig. 3E). Altogether, these results suggest that the anchorage of gp350 effectively improves the CD21$^+$ tumor targeting of RBC-EVs.

3.4. Chemotherapeutic drug-loaded RBC-EVs/gp350^{Etp} exhibit increased cytotoxicity to tumor CD21$^+$ B cells

Since RBC-EVs/gp350^{Etp} could effectively target CD21$^+$ tumors, understanding whether RBC-EVs/gp350^{Etp} loaded
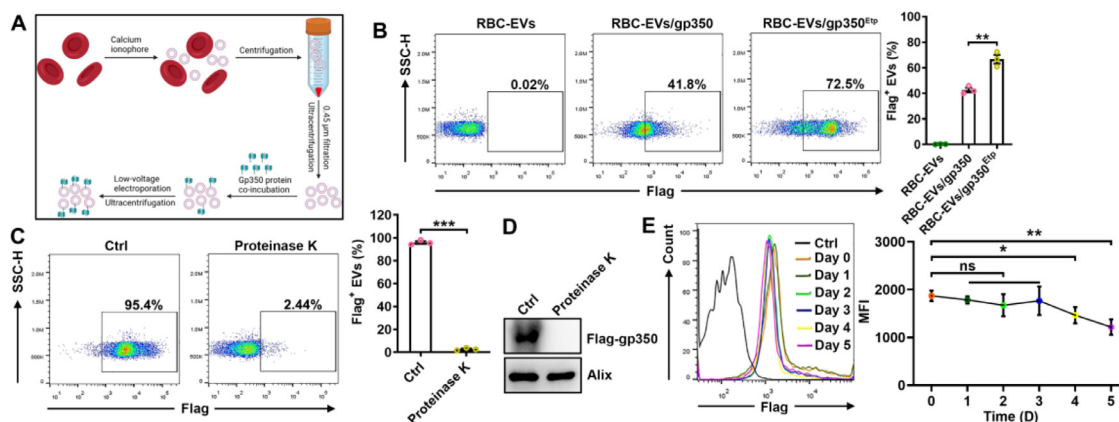
Fig. 2 – Successful anchorage of gp350 on RBC-EVs via the TM domain plus low-voltage electroporation. (A) Schematic diagram of the EV protein anchorage process. Briefly, 100 μg of RBC-EVs was incubated with 50 μg of purified gp350 protein for 60 min at 37 degrees Celsius, and this incubation was followed by electroporation at a voltage of 50 V. **(B)** RBC-EVs (100 μg) were incubated with 50 μg of purified gp350 proteins for 60 min at 37 degrees Celsius (RBC-EVs/gp350), and this incubation was followed by electroporation at a voltage of 50 V (RBC-EVs/gp350^{Etp}). Flow cytometry was employed to detect gp350 on RBC-EVs. **(C, D)** After treatment with 50 μg/ml proteinase K for 2 h, we measured gp350 on RBC-EVs/gp350^{Etp} by flow cytometry **(C)** or western blotting **(D)**. **(E)** After preservation at 37 degrees Celsius for the indicated time, gp350 on RBC-EVs/gp350^{Etp} was analyzed by flow cytometry. MFI, mean fluorescence intensity. ns, not significant; *$P < 0.05$, **$P < 0.01$ and ***$P < 0.001$ (unpaired Student's t test). Typical outcomes from three independent trials are given (mean ± SD) ($n = 3$).

with chemotherapeutic agents could be used to treat CD21$^+$ tumors such as BL and B-CLL is crucial. Dox and FA are common and effective drugs used for the treatment of BL and B-CLL [29,30]. Thus, we loaded Dox and FA into RBC-EVs and RBC-EVs/gp350^{Etp} (termed RBC-EVs/Dox, RBC-EVs/gp350^{Etp}/Dox, RBC-EVs/FA and RBC-EVs/gp350^{Etp}/FA, respectively). Because Dox has autofluorescence, we first measured Dox in EVs via flow cytometry and discovered that the RBC-EVs/Dox and RBC-EVs/gp350^{Etp}/Dox presented a similar MFI (Fig. S4A), which indicated the encapsulation of a similar amount of Dox. We also evaluated the drug loading efficiency of Dox and FA by high-performance liquid chromatography (HPLC). Based on the standard curve of Dox and FA, both RBC-EVs and RBC-EVs/gp350^{Etp} were loaded with similar amounts of Dox or FA (≈3 μg Dox or 17 μg FA for 100 μg RBC-EVs and RBC-EVs/gp350^{Etp}, respectively) (Fig. S4B-S4D). Consistent with our previous study [25], the loading of the drug had no influence on the integrity of the RBC-EVs but slightly increased their size (Fig. S4E and S4F).

We next evaluated the *in vitro* cytotoxicity of the drug-loaded RBC-EVs/gp350^{Etp}. As expected, RBC-EVs/gp350^{Etp}/Dox showed greater cytotoxicity in Raji cells than the same amounts of Dox (SA/Dox) and RBC-EVs/Dox, and the cytotoxicity was almost equal to that of RD/Dox at 72 h (Fig. 4A). However, the RBC-EVs/gp350^{Etp}/Dox and RBC-EVs/Dox had similar inhibitory effects on K562 cells (Fig. S5A). These results indicate that the increased cytotoxicity of RBC-EVs/gp350^{Etp}/Dox is dependent on CD21. Consistently, RBC-EVs/gp350^{Etp}/FA had greater cytotoxic activity against MEC-1 cells than the same amounts of FA (SA/FA) and

RBC-EVs/FA (Fig. 4B). Moreover, a flow cytometry analysis of apoptosis revealed that RBC-EVs/gp350^{Etp}/Dox and RBC-EVs/gp350^{Etp}/FA, but not RBC-EVs/Dox and RBC-EVs/FA, exerted more proapoptotic effects on Raji and MEC-1 cells, respectively (Fig. 4C and 4D). However, RBC-EVs/gp350^{Etp}/Dox and RBC-EVs/gp350^{Etp}/FA had similar proapoptotic effects on K562 cells (Fig. S5B). The above-described observations demonstrate that RBC-EVs/gp350^{Etp}/Dox and RBC-EVs/gp350^{Etp}/FA are more cytotoxic to tumor CD21$^+$ B cells *in vitro*.

3.5. Chemotherapeutic drug-loaded RBC-EVs/gp350^{Etp} exert stronger effects against BL and B-CLL

We subsequently examined the effects of RBC-EVs/gp350^{Etp}/Dox and RBC-EVs/gp350^{Etp}/FA against BL and B-CLL *in vivo*. First, we determined the optimal treatment dose of EVs and found that 100 μg RBC-EVs/gp350^{Etp}/Dox showed ideal treatment effects on Raji tumors compared with 150 μg RBC-EVs/gp350^{Etp}/Dox (Fig. S5C); thus, a dose of 100 μg was selected for subsequent experiments. The administration of SA/Dox and RBC-EVs/Dox had no inhibitory effect on the growth of Raji tumors, and RBC-EVs/gp350^{Etp}/Dox significantly inhibited Raji tumor growth to levels almost equal to those obtained with RD/Dox treatment (Fig. 5A). No difference in tumor size was found between the RBC-EVs/gp350^{Etp}/Dox and RD/Dox treatments, but RBC-EVs/gp350^{Etp}/Dox treatment significantly extended the survival of Raji tumor-bearing mice in compared with that obtained with RD/Dox treatment (Fig. 5B). TUNEL assays of tumor tissues showed that RBC-EVs/gp350^{Etp}/Dox treatment
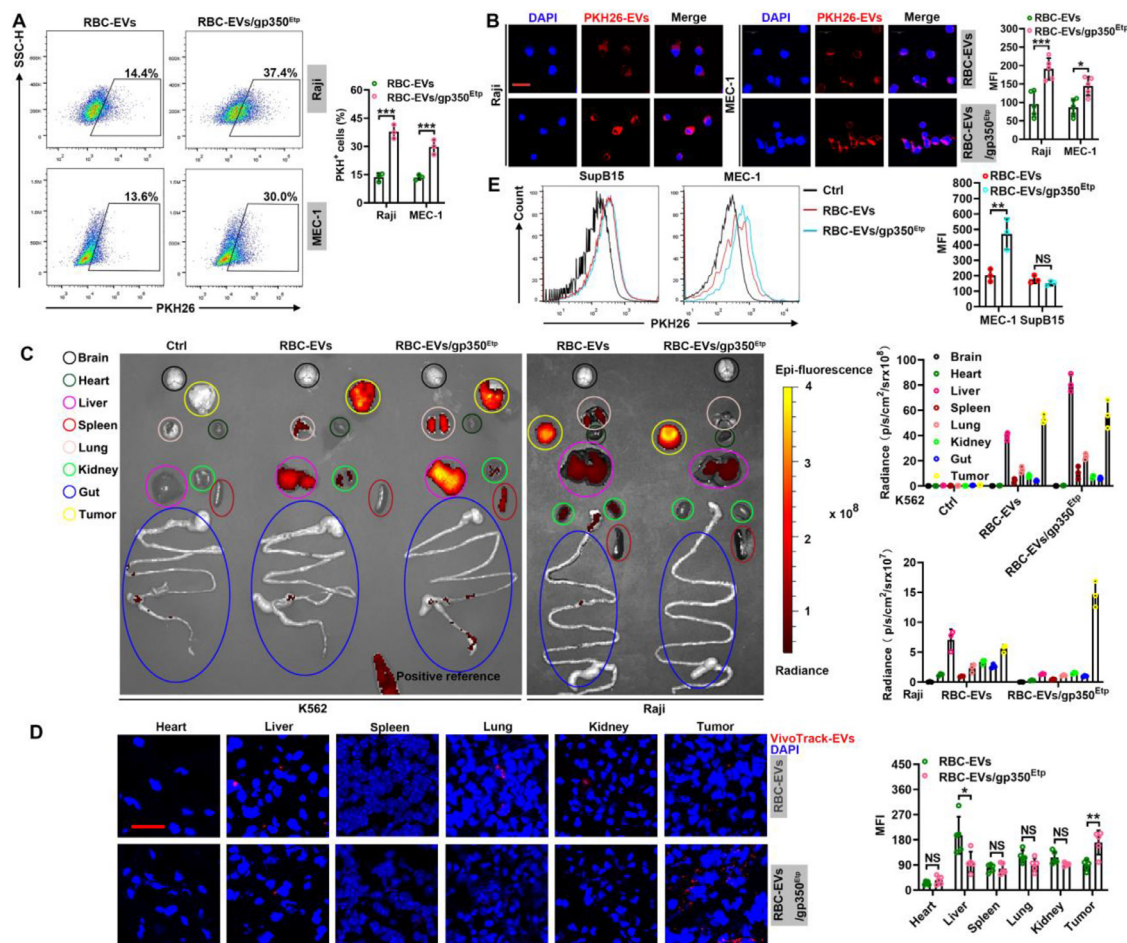
Fig. 3 – RBC-EVs/gp350^{Etp} show enhanced targeting to tumor CD21$^+$ B cells. (A, B) Raji or MEC-1 cells were maintained with 10 µg/ml PKH26-labeled RBC-EVs or RBC-EVs/gp350^{Etp} at 37 degrees Celsius for 1 h (A) or 4 h (B). The uptake of EVs was then detected by flow cytometry (A) and fluorescence microscopy (B). Scale bar, 20 µm in (B). **(C, D)** K562 or Raji tumor-bearing nude mice were injected i.v. with VivoTrack 680-labeled RBC-EVs or RBC-EVs/gp350^{Etp} (100 µg) for 1 d Typical *ex vivo* imaging and quantification of EV uptake in the indicated organs and tumors (C). Fluorescence microscopy detection of VivoTrack 680$^+$ cells in the indicated organ sections (D). Scale bar, 20 µm in (D). **(E)** NCG mice were inoculated i.v. with MEC-1 or SupB15 cells for 8 d and then injected i.v. with VivoTrack 680-labeled RBC-EVs or RBC-EVs/gp350^{Etp} (100 µg) for 1d. We then detected the MFI of MEC-1 or SupB15 tumor cells by flow cytometry analysis. ns, not significant; *$P < 0.05$, **$P < 0.01$ and ***$P < 0.001$ (unpaired Student's t test). Typical outcomes from three independent trials are given (mean ± SD) ($n = 3$-5).

led to a more notable increase in Raji cell apoptosis than no treatment and RBC-EVs/Dox treatment (Fig. 5C). However, this effect of RBC-EVs/gp350^{Etp}/Dox was significantly weaker than that of RD/Dox (Fig. 5C). Moreover, immunofluorescence staining of the proliferation marker Ki67 revealed that RBC-EVs/gp350^{Etp}/Dox treatment significantly reduced the proliferation of tumor cells, and this reduction was almost equal to that obtained with RD/Dox (Fig. 5C). Furthermore, we confirmed that cell death induced by RBC-EVs/gp350^{Etp}/Dox was related to the classical apoptotic pathway, as evidenced by a reduction in Bcl2 and an increase in cleaved caspase 3 in tumor tissues (Fig. 5D). The analysis of CD21$^-$ K562 tumors revealed that neither RBC-EVs/gp350^{Etp}/Dox nor RBC-EV/Dox exerted obvious inhibitory effects, whereas RD/Dox significantly inhibited the progression of these tumors (Fig.

S5D). Moreover, RD/Dox but not RBC-EVs/gp350^{Etp}/Dox and RBC-EV/Dox extended the survival time of K562 tumor-bearing mice (Fig. S5E).

We then evaluated the effects of RBC-EVs/gp350^{Etp}/FA against B-CLL by introducing MEC-1-Luci leukemia into NCG mice. More significant tumor suppression was observed in mice that received RBC-EVs/gp350^{Etp}/FA than in those that received RBC-EVs/FA, but this suppression was weaker than that obtained with RD/FA (Fig. 5E). In addition, significantly longer survival was observed among the RBC-EVs/gp350^{Etp}/FA- and RD/FA-treated mice (Fig. 5F). However, unlike the results found for the magnitude of tumor suppression, RBC-EVs/gp350^{Etp}/FA and RD/FA had similar effects on the survival of tumor-bearing mice (Fig. 5F). Collectively, the results demonstrate that Dox- or FA-loaded
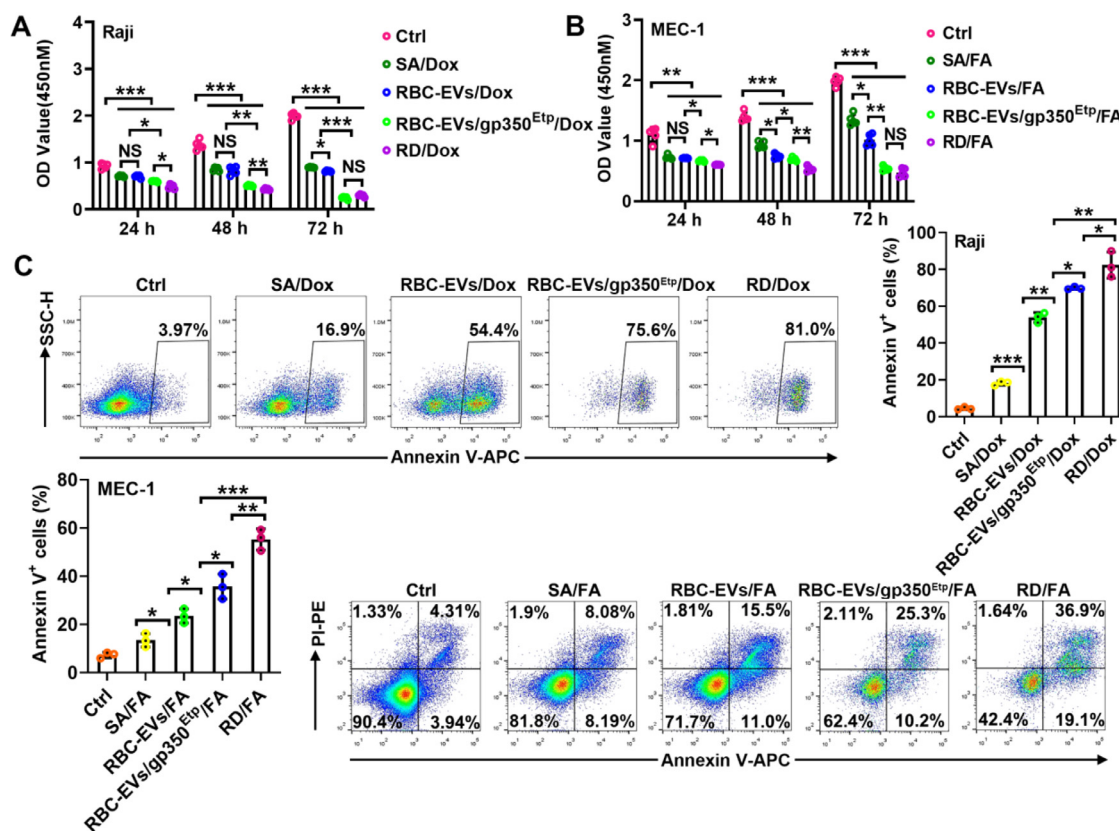
Fig. 4 – Chemotherapeutic drug-loaded RBC-EVs/gp350^{Etp} exhibit increased cytotoxicity to tumor CD21^{+} B cells. (A) After treatment with SA/Dox (0.3 µg/ml Dox), RBC-EVs/Dox, RBC-EVs/gp350^{Etp}/Dox, or RD/Dox (5 µg/ml Dox) for the indicated times, we measured the viability of Raji cells with CCK-8 assays. (B) After treatment with SA/FA (1.7 µg/ml FA), RBC-EVs/FA, RBC-EVs/gp350^{Etp}/FA, or RD/FA (10 µg/ml FA) for the indicated times, the MEC-1 cell viability was measured with CCK-8 assays. (C) After treatment with SA/Dox (0.3 µg/ml Dox), RBC-EVs/Dox, RBC-EVs/gp350^{Etp}/Dox, or RD/Dox (5 µg/ml Dox) for 24 h, we measured Raji cell apoptosis by flow cytometry utilizing an Annexin V staining kit. (D) After treatment with SA/FA (1.7 µg/ml FA), RBC-EVs/FA, RBC-EVs/gp350^{Etp}/FA, or RD/FA (10 µg/ml FA) for 1 d, the apoptosis rate of MEC-1 cells was determined via flow cytometry utilizing an Annexin V/PI staining kit. ns, not significant; *$P < 0.05$; **$P < 0.01$ and ***$P < 0.001$ (one-way ANOVA followed by Newman–Keuls multiple comparison test). Typical outcomes from three independent trials are given (mean ± SD) ($n = 3$).

RBC-EVs/gp350^{Etp} are effective in treating CD21^{+} BL and B-CLL.

3.6. Drug toxicity evaluation of RBC-EVs/gp350^{Etp}/Dox and RBC-EVs/gp350^{Etp}/FA

To investigate the potential clinical application of RBC-EVs/gp350^{Etp}/Dox and RBC-EVs/gp350^{Etp}/FA, we further assessed the toxicity of RBC-EVs/gp350^{Etp}/Dox and RBC-EVs/gp350^{Etp}/FA *in vivo*. RBC-EVs/gp350^{Etp}/Dox did not cause severe weight loss, whereas RD/Dox did exert this effect (Fig. 6A). Cardiotoxicity is the major side effect associated with Dox [37,38]. Thus, we evaluated the CK-MB and LDH levels in sera because these compounds are marker enzymes of myocardial damage [39]. Marked increases in the serum CK-MB and LDH levels were observed in the RD/Dox-treated mice but not RBC-EVs/gp350^{Etp}/Dox-treated mice (Fig. 6B). Furthermore, the RBC-EVs/gp350^{Etp}/Dox-treated mice showed

no obvious histopathological damage in the five main organs stated previously, and the same was true for the RD/Dox-treated mice with the exception of marked heart damage (Fig. 6C). Another side effect of the clinical use of Dox is systemic myelosuppression, which limits intensification of its dose [40,41]. As expected, the leukocyte and RBC numbers were markedly decreased in the RD/Dox-treated mice, whereas the numbers of both of these cells remained unchanged in the RBC-EVs/gp350^{Etp}/Dox-treated mice (Fig. 6D). In addition, Dox can induce the release of a vast number of inflammatory cytokines [42]. Indeed, RD/Dox treatment greatly increased the serum levels of proinflammatory cytokines, including IL-1β, IL-6 and TNF, whereas RBC-EVs/gp350^{Etp}/Dox did not obviously alter the serum levels of these cytokines (Fig. 6E). FA reportedly causes myelosuppression [43], autoimmune hemolytic anemia [44] and eosinophilia [45]. RD/FA but not RBC-EVs/gp350^{Etp}/FA reduced the blood leukocyte numbers, which indicated that RD/FA induces myelosuppression (Fig.
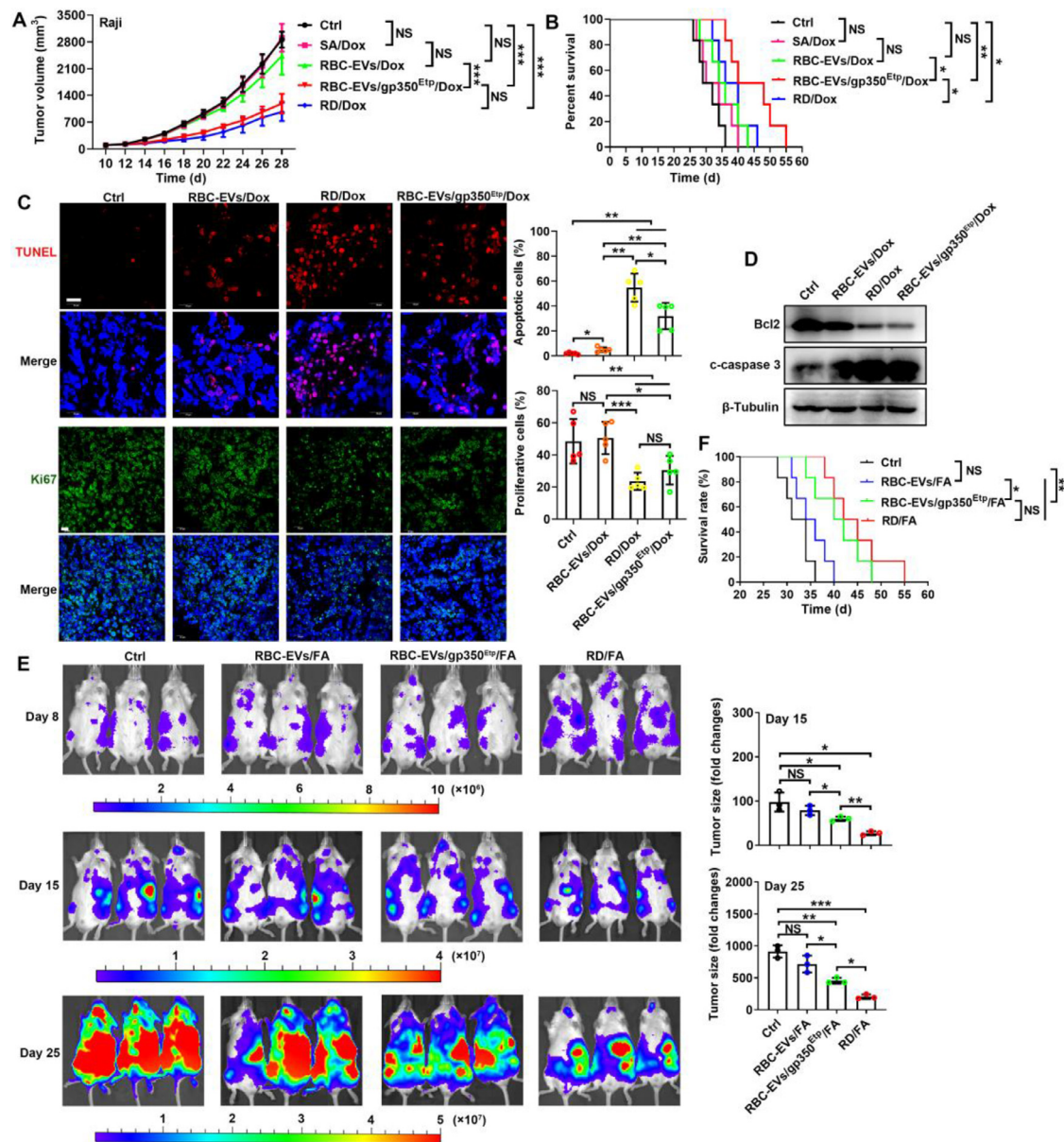
Fig. 5 – Chemotherapeutic drug-loaded RBC-EVs/gp350^{Etp} exert stronger effects against BL and B-CLL. (A-D) 7 d after injection with 1×10^7 Raji cells, mice were injected i.v. with RBC-EVs (100 μg), RBC-EVs/Dox (100 μg), SA/Dox (3 μg Dox), RD/Dox (5 mg/kg Dox) or 100 μg of RBC-EVs/gp350^{Etp}/Dox every 3 d. Tumor progression was evaluated based on the tumor size (A) and survival time (B). Representative images of TUNEL and Ki67 immunofluorescence staining of tumor tissues from mice subjected to the indicated treatment for 10 d are shown (left) and were statistically analyzed (right). Scale bars, 20 μm (C). WB analysis of Bcl2 and cleaved caspase 3 (c-caspase 3) proteins in tumor tissues from mice subjected to the indicated treatment for 10 d (D). (E, F) NCG mice were injected i.v. with 2×10^6 MEC-1-Luci cells, and 8 d later, the mice were injected i.v. with 100 μg RBC-EVs, 100 μg RBC-EVs/FA, 100 μg RBC-EVs/gp350^{Etp}/FA or RD/FA (25 mg/kg FA) every 3 d. The tumors were monitored via IVIS on Days 8, 15 and 25 (left). We evaluated tumor progression by computing the tumor signal intensity on Day 15 or 25 divided by that on Day 8 (right) (E) and based on the survival (F). ns, not significant; *P < 0.05; **P < 0.01 and ***P < 0.001 (one-way ANOVA followed by Newman–Keuls multiple comparison test). Typical outcomes from three independent trials are given (mean ± SD) ($n = 3$-7).

6F). However, in our model, we did not observe any significant changes in blood RBCs, hemoglobin or eosinophils in the mice administered RD/FA or RBC-EVs/gp350^{Etp}/FA (Fig. 6F). To consider their future clinical applications, we also tested the cytotoxicity of RBC-EVs/gp350^{Etp}/FA to CD21$^+$ lymphocytes.

We found that although RBC-EVs/gp350^{Etp}/FA greatly induced the apoptosis of MEC-1 cells, they exhibited almost no cytotoxicity to CD21$^+$ lymphocytes (Fig. 6G), which was probably caused by a reduced uptake of RBC-EVs/gp350^{Etp}/FA by CD21$^+$ lymphocytes than by MEC-1 cells (Fig. S6A and S6B).
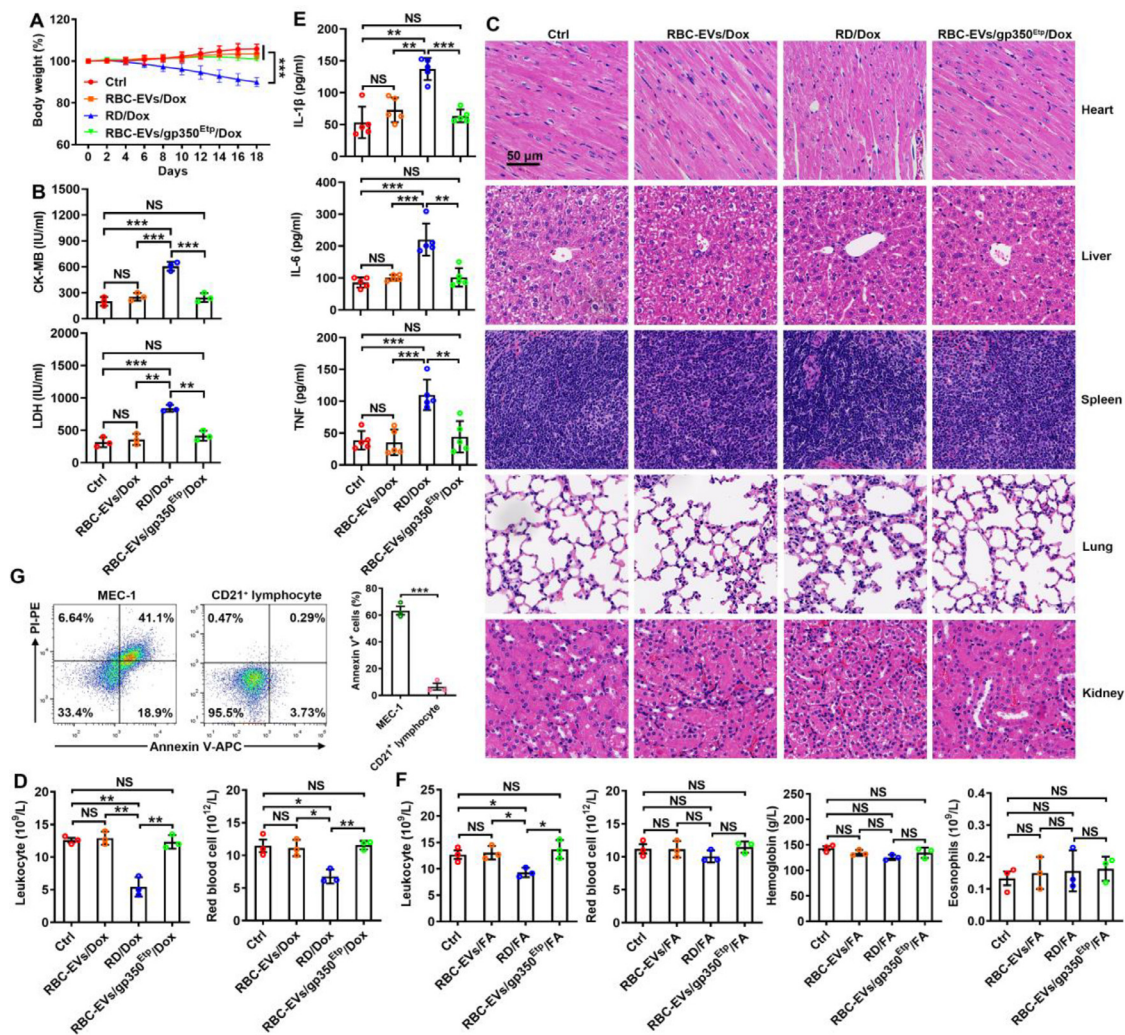
Fig. 6 – Drug toxicity evaluation of RBC-EVs/gp350^{Etp}/Dox and RBC-EVs/gp350^{Etp}/FA. (A-E) C57BL/6J mice were treated with RBC-EVs/gp350^{Etp}/Dox (100 μg) or RD/Dox (5 mg/kg Dox) every 3 d. The body weights were recorded every other day (A). The serum LDH and CK-MB levels were measured after 10 d (B). Representative images of five major organs (H&E stained) after 18 d. Scale bar, 50 μm (C). Blood leukocytes and RBCs (D) and serum inflammatory cytokines (IL-1β, IL-6 and TNF) (E) were detected after 10 d. (F) C57BL/6J mice were treated with RBC-EVs/gp350^{Etp}/FA (100 μg) or RD/FA (25 mg/kg FA) every 3 d. The numbers of blood leukocytes, RBCs, and eosinophils and the hemoglobin levels were measured after 10 d. (G) MEC-1 cells or CD21$^+$ lymphocytes were cultured with or without 10 μg/ml RBC-EVs/gp350^{Etp}/FA at 37 degrees Celsius for 12 h. The apoptosis of cells was measured by flow cytometry using an Annexin V-PI staining kit. ns: not significant; *$P < 0.05$; **$P < 0.01$ and ***$P < 0.001$ (one-way ANOVA followed by Newman–Keuls multiple comparison test). Typical outcomes from three independent trials are given (mean ± SD) ($n = 3$-5).

Thus, these data suggest that RBC-EVs/gp350^{Etp}/Dox and RBC-EVs/gp350^{Etp}/FA have satisfactory biosafety.

4. Conclusion

Here, we directly anchored gp350 onto RBC-EVs via its TM region and utilized the characteristic that gp350 specifically binds to CD21 on B cells to make RBC-EVs that target CD21$^+$ B cell tumors. We combined this approach with low-voltage electroporation to further improve the anchoring efficiency of gp350. After loading with Dox or FA, RBC-EVs/gp350^{Etp} showed powerful cytotoxicity to BL or B-CLL, respectively. Unlike CAR T cells, which cause deadly cytokine release syndrome, drug-loaded RBC-EVs/gp350^{Etp} possess excellent safety and thus show notable therapeutic effects on these malignancies.

In conclusion, this study established a new strategy to efficiently anchor gp350 onto RBC-EVs. BL or B-CLL, whose therapy remains challenging, could be effectively inhibited by gp350-anchored RBC-EVs loaded with Dox or FA, respectively. Hence, our findings will contribute to the exploration of new strategies for BL and B-CLL therapy.

Conflicts of interest

Acknowledgements

Supplementary materials

Supplementary material associated with this article can be found, in the online version, at doi:10.1016/j.ajps.2022.03.004.

REFERENCES

[1] Gill S, June CH. Going viral: chimeric antigen receptor T-cell therapy for hematological malignancies. Immunol Rev 2015;263(1):68–89.

[2] Haslauer T, Greil R, Zaborsky N, Geisberger R. CAR T-cell therapy in hematological malignancies. Int J Mol Sci 2021;22(16):8996.

[3] Brentjens RJ, Davila M L, Riviere I, Park J, Wang X, Cowell LG, et al. CD19-targeted T cells rapidly induce molecular remissions in adults with chemotherapy-refractory acute lymphoblastic leukemia. Sci Transl Med 2013;5(177):177ra38.

[4] Dai H, Wu Z, Jia H, Tong C, Guo Y, Ti D, et al. Bispecific CAR-T cells targeting both CD19 and CD22 for therapy of adults with relapsed or refractory B cell acute lymphoblastic leukemia. J Hematol Oncol 2020;13(1):30.

[5] Zhou X, Ge T, Li T, Huang L, Cao Y, Xiao Y, et al. CAR19/22 T cell therapy in adult refractory Burkitt's lymphoma. Cancer Immunol Immunother 2021;70(8):2379–84.

[6] Vitale C, Strati P. CAR T-cell therapy for B-cell non-Hodgkin lymphoma and chronic lymphocytic leukemia: clinical trials and real-world experiences. Front Oncol 2020;10:849.

[7] Riches JC, Davies JK, McClanahan F, Fatah R, Iqbal S, Agrawal S, et al. T cells from CLL patients exhibit features of T-cell exhaustion but retain capacity for cytokine production. BLOOD 2013;121(9):1612–21.

[8] Zhou Q, Munger ME, Highfill SL, Tolar J, Weigel BJ, Riddle M, et al. Program death-1 signaling and regulatory T cells collaborate to resist the function of adoptively transferred cytotoxic T lymphocytes in advanced acute myeloid leukemia. Blood 2010;116(14):2484–93.

[9] Cosenza M, Sacchi S, Pozzi S. Cytokine release syndrome associated with T-cell-based therapies for hematological malignancies: pathophysiology, clinical presentation, and treatment. Int J Mol Sci 2021;22(14):7652.

[10] Lemal R, Tournilhac O. State-of-the-art for CAR T-cell therapy for chronic lymphocytic leukemia in 2019. Journal for immunotherapy of cancer 2019;7(1):202.

[11] Avigdor A, Shouval R, Jacoby E, Davidson T, Shimoni A, Besser M, et al. CAR T cells induce a complete response in refractory Burkitt Lymphoma. Bone Marrow Transplant 2018;53(12):1583–5.

[12] Gudbergsson JM, Jønsson K, Simonsen JB, Johnsen KB. Systematic review of targeted extracellular vesicles for drug delivery - Considerations on methodological and biological heterogeneity. J Control Release 2019;306:108–20.

[13] van Niel G, D'Angelo G, Raposo G. Shedding light on the cell biology of extracellular vesicles. Nat Rev Mol Cell Biol 2018;19(4):213–28.

[14] Sun H, Burrola S, Wu J, Ding WQ. Extracellular vesicles in the development of cancer therapeutics 2020;21(17):6097.

[15] Chen L, Hong W. Recent progress in targeted delivery vectors based on biomimetic nanoparticles. Signal Transduct Target Ther 2021;6(1):225.

[16] Poggio M, Hu T, Pai CC, Chu B, Belair CD, Chang A, et al. Suppression of exosomal PD-L1 induces systemic anti-tumor immunity and memory. Cell 2019;177(2):414–27.

[17] Wang H, Zhou Y, Sun Q, Zhou C, Hu S, Lenahan C, et al. Update on Nanoparticle-Based Drug Delivery System for Anti-inflammatory Treatment. Front Bioeng Biotechnol 2021;9:630352.

[18] Yao X, Lyu P, Yoo K, Yadav MK, Singh R, Atala A, et al. Engineered extracellular vesicles as versatile ribonucleoprotein delivery vehicles for efficient and safe CRISPR genome editing. J Extracell Vesicles 2021;10(5):e12076.

[19] Tian Y, Li S, Song J, Ji T, Zhu M, Anderson GJ, et al. A doxorubicin delivery platform using engineered natural membrane vesicle exosomes for targeted tumor therapy. Biomaterials 2014;35(7):2383–90.

[20] Elsharkasy OM, Nordin JZ, Hagey DW, de Jong OG, Schiffelers RM, Andaloussi SE, et al. Extracellular vesicles as drug delivery systems: Why and how? Adv Drug Deliv Rev 2020;159:332–43.

[21] Witwer KW, Wolfram J. Extracellular vesicles versus synthetic nanoparticles for drug delivery. Nature Reviews Materials 2021;6(2):103–6.

[22] Kamerkar S, LeBleu VS, Sugimoto H, Yang S, Ruivo C F, Melo S A, et al. Exosomes facilitate therapeutic targeting of oncogenic KRAS in pancreatic cancer. Nature 2017;546(7659):498–503.

[23] Choi H, Kim Y, Mirzaaghasi A, Heo J, Kim YN, Shin J H, et al. Exosome-based delivery of super-repressor $I\kappa B\alpha$ relieves sepsis-associated organ damage and mortality. Science Advances 2020;6(15):eaaz6980.

[24] Usman WM, Pham TC, Kwok YY, Vu LT, Ma V, Peng B, et al. Efficient RNA drug delivery using red blood cell extracellular vesicles. Nature Communication 2018;9(1):2359.

[25] Zhang G, Huang X, Xiu H, Sun Y, Chen J, Cheng G, et al. Extracellular vesicles: natural liver-accumulating drug delivery vehicles for the treatment of liver diseases. J Extracell Vesicles 2020;10(2):e12030.

[26] Fingeroth J D, Weis JJ, Tedder TF, Strominger JL, Biro PA, Fearon DT. Epstein-Barr virus receptor of human B lymphocytes is the C3d receptor CR2. Proc Natl Acad Sci USA 1984;81(14):4510–4.

[27] Vallhov H, Gutzeit C, Johansson SM, Nagy N, Paul M, Li Q, et al. Exosomes containing glycoprotein 350 released by EBV-transformed B cells selectively target B cells through CD21 and block EBV infection *in vitro*. J Immunol 2011;186(1):73–82.

[28] Ruiss R, Jochum S, Mocikat R, Hammerschmidt W, Zeidler R. EBV-gp350 confers B-cell tropism to tailored exosomes and is a neo-antigen in normal and malignant B cells–a new option for the treatment of B-CLL. PLoS One 2011;6(10):e25294.

[29] Reiter A, Klapper W. Recent advances in the understanding and management of diffuse large B-cell lymphoma in children. Br J Haematol 2008;142(3):329–47.

[30] Montillo M, Ricci F, Tedeschi A. Role of fludarabine in hematological malignancies. Expert Rev Anticancer Ther 2006;6(9):1141–61.

[31] Hu Y, Kienlen-Campard P, Tang TC, Perrin F, Opsomer R, Decock M, et al. β-Sheet structure within the extracellular domain of C99 regulates amyloidogenic processing. Scientific reports 2017;7(1):17159.

[32] Wei G, Xiao S, Si D, Liu C. Improved HPLC method for doxorubicin quantification in rat plasma to study the pharmacokinetics of micelle-encapsulated and liposome-encapsulated doxorubicin formulations. Biomed Chromatogr 2008;22(11):1252–8.

[33] Puy JY, Jordheim LP, Cros-Perrial E, Dumontet C, Peyrottes S. Lefebvre-Tournier I. Determination and quantification of intracellular fludarabine triphosphate, cladribine triphosphate and clofarabine triphosphate by LC-MS/MS in human cancer cells. J Chromatogr B Analyt Technol Biomed Life Sci 2017;1053:101–10.

[34] Wan S, Wang S, Weng L, Zhang G. CD8alpha(+)CD11c(+) Extracellular vesicles in the lungs control immune homeostasis of the respiratory tract via TGF-beta1 and IL-10. J Immunol 2018;200(5):1651–60.

[35] Xiu F, Cai Z, Yang Y, Wang X, Wang J, Cao X. Surface anchorage of superantigen SEA promotes induction of specific antitumor immune response by tumor-derived exosomes. J Mol Med (Berl) 2007;85(5):511–21.

[36] Alex A, Piano V. Electroporated recombinant proteins as tools for *in vivo* functional complementation, imaging and chemical biology. Elife 2019;8:e48287.

[37] Chotenimitkhun R, D'Agostino RJ, Lawrence JA, Hamilton CA, Jordan JH, Vasu S, et al. Chronic statin administration may attenuate early anthracycline-associated declines in left ventricular ejection function. Can J Cardiol 2015;31(3):302–7.

[38] Wenningmann N, Knapp M, Ande A, Vaidya TR. Ait-Oudhia S. Insights into doxorubicin-induced cardiotoxicity: molecular mechanisms, preventive strategies, and early monitoring. Mol Pharmacol 2019;96(2):219–32.

[39] Danese E, Montagnana M. An historical approach to the diagnostic biomarkers of acute coronary syndrome. Ann Transl Med 2016;4(10):194.

[40] Fan M, Wen Y, Ye D, Jin Z, Zhao P, Chen D, et al. Acid-responsive H(2) -releasing 2D MgB(2) nanosheet for therapeutic synergy and side effect attenuation of gastric cancer chemotherapy. Adv Healthc Mater 2019;8(13):e1900157.

[41] Lucas A, Lam D, Cabrales P. Doxorubicin-loaded red blood cells reduced cardiac toxicity and preserved anticancer activity. Drug Delivery 2019;26(1):433–42.

[42] Maayah ZH, Alam AS, Takahara S, Soni S, Ferdaoussi M, Matsumura N, et al. Resveratrol reduces cardiac NLRP3-inflammasome activation and systemic inflammation to lessen doxorubicin-induced cardiotoxicity in juvenile mice. FEBS Lett 2021;595(12):1681–95.

[43] Rummel M, Kaiser U, Balser C, Stauch M, Brugger W, Welslau M, et al. Bendamustine plus rituximab versus fludarabine plus rituximab for patients with relapsed indolent and mantle-cell lymphomas: a multicentre, randomised, open-label, non-inferiority phase 3 trial. Lancet Oncol 2016;17(1):57–66.

[44] Nishida H, Murase T, Ueno H, Park JW, Yano T, Ikeda Y. Fludarabine-associated autoimmune hemolytic anemia occurring in B-cell chronic lymphocytic leukemia. Leuk Res 2006;30(12):1589–90.

[45] Voutsadakis IA. Fludarabine-induced eosinophilia: case report. Ann Hematol 2002;81(5):292–3.